Spin-polarized resonant transport in a hybrid ferromagnetic–two-dimensional electron gas structure

S. Bala Kumar,[1,2] M. B. A. Jalil,[1] and S. G. Tan[2]
[1]*Information Storage Materials Lab, Electrical & Computer Engineering Department, National University of Singapore, Singapore 117576*
[2]*Data Storage Institute, DSI Building, 5 Engineering Drive 1, Off Kent Ridge Crescent, National University of Singapore, Singapore 117608*

(Received 21 September 2006; revised manuscript received 5 January 2007; published 6 April 2007)

We investigated the spin-polarized resonant transport in a hybrid high-electron-mobility transistor (HEMT) structure, with source and drain electrodes made of ferromagnetic (FM) material, while the channel consists of a highly doped n^{++} AlGaAs-GaAs two-dimensional electron gas (2DEG). The electron transport in the FM layer is modeled using the spin-drift diffusion model, while across the 2DEG layer, ballistic transport is assumed, given the long mean free path within the 2DEG. By solving the two transport models self-consistently, we found that the transport properties of the device, such as the transmission probability, the spin injection (SI) efficiency, and the magnetoresistance (MR) ratio, all exhibit oscillatory behavior when the 2DEG layer width or the 2DEG Fermi energy is varied. The basis of these oscillations is the resonant transport across the 2DEG, which is reminiscent of the spin-polarized resonant tunneling (SPRT), observed recently in magnetic tunnel junctions (MTJs). The hybrid device has distinct advantages over the metal-based MTJ structures in the practical utilization of the SPRT effect. This is because the ballistic charge conduction through the 2DEG enables easy tunability of the MR ratio and SI efficiency, by varying the doping density and gate bias, while avoiding the exponential suppression of MR with barrier thickness, which occurs in MTJ devices. Numerically, the hybrid HEMT device is predicted to be capable of achieving maximum MR and SI ratios approaching 20% and 40%, respectively, at the crest of their respective oscillations.

DOI: 10.1103/PhysRevB.75.155309 PACS number(s): 85.75.−d

I. INTRODUCTION

Spintronics is a rapidly emerging field that promises to provide new advances with substantial impact for future applications.[1–4] In particular, semiconductor- (SC-) based spintronics[3] can combine the well-known advantages of SC materials (i.e., versatility of charge transport manipulation and established nanofabrication technology) with the additional functionality provided by the spin degree of freedom. Recent experimental demonstrations of long spin coherence length[5,6] in SCs and the ability to manipulate spin orientation by electrical and magnetic means[7–10] have brought the possibility of SC-based spintronics devices for memory, optoelectronic, and spin-field-effect transistor applications[11] closer to realization. Two key parameters which need to be optimized in future SC-based spintronic devices are (i) its spin injection (SI) efficiency, i.e., the ability to inject spin-polarized current into a semiconductor,[12–14] and (ii) the magnetoresistance (MR) ratio. Initial SC-based devices which utilized direct spin injection from ferromagnetic (FM) metal electrodes into the SC layer had extremely low SI and MR ratios due to the large conductivity mismatch.[15–19] This mismatch problem has been overcome by the incorporation of tunnel barriers[16,20] and the use of diluted magnetic semiconductors (DMSs) as spin injectors,[7] although the latter suffer from a generally low Curie temperature.[7,22]

Recently, quantum effects resulting in resonant oscillatory MR behavior have also been experimentally observed and theoretically predicted in double-barrier structures based on DMSs[23] and hybrid FM-SC materials,[24] respectively. Such oscillatory behavior may potentially be utilized to manipulate and optimize the MR and SI ratios in SC-based devices, as well as provide additional functionalities, such as spin-dependent resonant tunneling devices in the coherent tunneling regime. The oscillatory MR behavior was first observed in magnetic tunnel junctions (MTJs), where a thin nonmagnetic (NM) metal layer is inserted in between the insulating tunnel barrier and one of the FM metal electrodes.[25] The effect is ascribed to the spin-polarized resonant tunneling (SPRT) effect involving quantum well states and exhibits tunneling MR (TMR) oscillations as the NM layer is varied. Theoretically, the SPRT effect was first modeled by single-band models,[26,27] which demonstrate a nonzero TMR in the presence of the NM insertion, thus contradicting the classical theory of tunneling. Subsequently, Mathon and Umerski[28] provided a more refined theoretical model of SPRT by incorporating more realistic band structures. Experimentally, various studies have been conducted to investigate the SPRT effect in metal MTJ structures.[25,29,31–35] However, the SPRT oscillatory effect is found to be small[25,30,35] or virtually unobservable.[29,31–34] Although the use of double-MTJ structures[36] may enhance some of the quantum size effects, there are key obstacles to its realization in metal-based MTJs: (i) the TMR ratio decays rapidly (exponentially) with increasing thickness of the NM insertion, (ii) the oscillatory frequency is very high with a modulation period of only $\sim 1-2$ nm, given the large Fermi wave vector in the NM metal insertion, and (iii) there appears to be only one (rather inconvenient) method to modulate the TMR modulation, i.e., by changing the NM thickness.[25,29,30,35,36]

Thus, to overcome these difficulties, we propose the utilization of a hybrid high-electron-mobility transistor

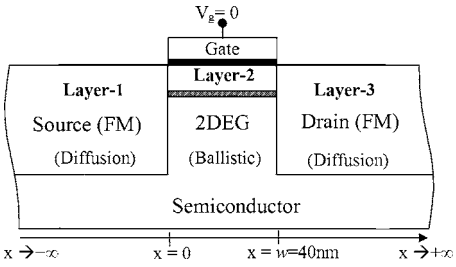

FIG. 1. Schematic illustration of the hybrid SC-FM device based on the HEMT. It consists of a 2DEG conducting channel between FM source and drain electrodes.

(HEMT) structure, with source and drain made of FM material, as shown in Fig. 1, to achieve the SPRT effect. The channel of the HEMT structure consists of a highly doped n^{++} AlGaAs-GaAs two-dimensional electron gas (2DEG) layer. Electron transport in the FM layer is modeled using the spin-drift diffusion (SDD) model, in which the electron undergoes momentum and spin scattering while traveling inside the FM layers. In the 2DEG layer, electron transmission is modeled as ballistic transmission, where the electron is transmitted across the layer without any scattering. Spin polarization and momentum are preserved during this transmission. Ballistic transmission in the 2DEG layer is achieved by ensuring that the thickness of the layer is smaller than the mean free path of electron in the layer. The ballistic transport yields an oscillatory behavior, reminiscent of the SPRT effect. Utilizing the SPRT effect may provide a potential method of optimizing the MR ratio of the device—e.g., by setting the lateral dimension of the device to coincide with one of the resonant MR peaks. The key advantages of this oscillatory MR effect in SCs as opposed to metallic MTJ devices are that (i) ballistic transport can occur in the free conduction instead of tunneling regimes, so that the transmission probability is not exponentially suppressed with the barrier width, (ii) the low Fermi wave vector in the 2DEG allows for a larger modulation period and hence obviates the need for precise optimization of the 2DEG thickness, and (iii) the use of the versatile 2DEG material allows for other avenues of MR modulation. For instance, the MR ratio can be tuned or controlled externally either by application of a gate bias or by changing the 2DEG doping level, thus providing an added functionality compared to the usual metallic spin-valve devices. Numerically, our self-consistent calculations yield significant MR and SI ratios, which approach 20% and 40%, respectively, at the peak of the oscillations.

II. THEORY

A. Spin drift-diffusive transport in the FM electrodes

We first present the spin transport model within the FM source and drain electrodes. Throughout this paper, λ_i, α_i, ρ_i, β_i, A_i, and j_i indicate the spin diffusion length, intrinsic conductance polarization, resistivity, current polarization, cross-sectional area, and current density of layer i, respectively. w refers to the width of the 2DEG layer. The subscript and superscript $\uparrow$ ($\downarrow$) represent the majority (minority) spin component, while the subscript S (F) refers to the semiconductor 2DEG (FM) layer. Our spin transport model is essentially a 1D approximation, with x taken to be the spatial variable. It has been assumed there is no significant variation of the current and potential in the transverse y direction.

Within the FM layers, the conduction electrons encounter spin-asymmetric scattering processes. The corresponding electron transport can be modeled by the well-established semiclassical SDD model.[16,37,38] For simplicity, we consider the case of collinear magnetization—i.e., the magnetization of the FM layers are in parallel or antiparallel orientations—but in principle our analysis can be extended to the more general noncollinear case—e.g., via a scattering matrix or generalized Boltzmann formalisms.[39,40] In our model, we set the total current $I=jA$ to be some constant value and consider the variation of the electrochemical potential across the device. Due to the spin-dependent scattering in the FM layers, the spin-dependent components of j_F and ρ_F can be expressed by

$$j_{F\uparrow} = \beta j_F, \quad j_{F\downarrow} = (1-\beta) j_F, \tag{1a}$$

$$\rho_{F\uparrow} = 2\rho_F/(1+\alpha_F), \quad \rho_{F\downarrow} = 2\rho_F/(1-\alpha_F), \tag{1b}$$

where $\rho_{F\uparrow} \| \rho_{F\downarrow} = \rho_F$ and $j_{F\uparrow} + j_{F\downarrow} = j_F$. α_F is an intrinsic property of the FM material, while the spin polarization of current $\beta(x)$ is a spatially varying quantity, which is to be determined. Based on Ohm's law, the electrochemical potential gradient is given by

$$\frac{\partial \mu_{\uparrow,\downarrow}}{\partial x} = -e\rho_{\uparrow,\downarrow} j_{\uparrow,\downarrow}, \tag{2}$$

where μ is the electrochemical potential, e is the electron charge, and x is the spatial position. Spin accumulation which arises from the spin split in the electrochemical potential, i.e., $\Delta\mu = \mu_\uparrow - \mu_\downarrow$, varies according to a second-order diffusion equation

$$\frac{\partial^2 \Delta\mu}{\partial x^2} = \frac{\Delta\mu}{\lambda^2}.$$

The general solution for the spin accumulation $\Delta\mu_i(x)$ in the FM electrodes (i.e., layers $i=1$ and 3) can be expressed as

$$\Delta\mu_i(x) = P_i \exp\left(\frac{x}{\lambda_i}\right) + Q_i \exp\left(-\frac{x}{\lambda_i}\right). \tag{3}$$

The coefficients P_1, Q_1, P_3, and Q_3 can be solved by applying the following boundary conditions at the FM-2DEG interfaces ($x=0$ and $x=w$):

$$e j_\uparrow(0)\rho_{1\uparrow} - e j_\downarrow(0)\rho_{1\downarrow} = -\left.\frac{\partial \Delta\mu_1(x)}{\partial x}\right|_{x=0}, \tag{4}$$

$$e j_\uparrow(w)\rho_{3\uparrow} - e j_\downarrow(w)\rho_{3\downarrow} = -\left.\frac{\partial \Delta\mu_3(x)}{\partial x}\right|_{x=w}, \tag{5}$$

and at the terminals of the semi-infinite FM contacts ($x = \pm\infty$), where spin accumulation vanishes,

$$\Delta\mu_1(x \to -\infty) = \Delta\mu_3(x \to +\infty) = 0. \tag{6}$$

Additionally, the continuity of the electrochemical potentials dictates that

$$\Delta\mu_3(w) - \Delta\mu_1(0) = -(\Delta U_2^{\uparrow} - \Delta U_2^{\downarrow}), \tag{7}$$

where $\Delta U_2^{\downarrow,\uparrow}$ refers to the electrochemical potential drop of spin-up (-down) current across the 2DEG layer. Equations (4) and (5) are derived from Eq. (2) by considering the spin current at the interfaces. Due to ballistic transmission, we assume no spin flip scattering in the 2DEG layer, and thus $j_{\uparrow,\downarrow}(0) = j_{\uparrow,\downarrow}(w)$. Solving the above boundary conditions—i.e., Eqs. (4)–(7) simultaneously—yields the following expressions for P_1, Q_1, P_3, and Q_3 and the current polarization at the two FM-2DEG interfaces $\beta(0)$ and $\beta(w)$:

$$P_1 = \frac{\Delta U_2^{\uparrow} - \Delta U_2^{\downarrow}}{2}, \tag{8a}$$

$$Q_3 = \frac{e^{w/\lambda_F}(\Delta U_2^{\downarrow} - \Delta U_2^{\uparrow})}{2}, \tag{8b}$$

$$Q_1 = P_3 = 0, \tag{8c}$$

$$\beta(0) = \beta(w) = \frac{(1+\alpha_F)}{2}\left(\frac{(1-\alpha_F)(\Delta U_2^{\uparrow} - \Delta U_2^{\downarrow})}{4ej_F\lambda_F\rho_F} + 1\right). \tag{8d}$$

Note that $\beta(0) = \beta(w)$ due to the absence of spin flip in the 2DEG layer. From the above results, the spatial variation of spin accumulation $\Delta\mu$ in Eq. (3) can be determined. Subsequently, the spatial profile of $\beta(x)$ across FM layers are obtained by considering Eqs. (4) and (5) for an arbitrary position x. The solution $\beta_i(x)$ is then substituted into Eqs. (1) and (2), and after integration, the spatial dependence of the electrochemical potential for both spins, $\mu_{\uparrow,\downarrow}(x)$, is obtained within each FM layer.

To analyze the MR, we let layer 1 be the pinned FM layer with a fixed magnetization, while layer 3 is the free FM layer, whose magnetization orientation can be switched by an external field. The solutions in Eqs. (8a)–(8d) apply for the case of parallel (P) configuration. We repeat the above analysis for the antiparallel (AP) configuration, where the magnetization of layer 3 is in the opposite direction to that of layer 1. The spin-dependent resistivities of the FM layers in the P and AP configurations, $\rho_{F\uparrow,\downarrow}^{P(AP)}$, are related to one another as follows:

$$\rho_{F\uparrow,\downarrow} = \rho_{F\uparrow,\downarrow}^{P} = \rho_{F\downarrow,\uparrow}^{AP}. \tag{9}$$

In computing the MR ratio, we consider the electrochemical potential drop between $x = -\lambda_F$ and $x = w + \lambda_F$, i.e., a thickness of λ_F in each of the FM contacts. This is because λ_F is the length scale across which the spin-dependent resistance changes will occur.[15] The explicit expression for MR is given by

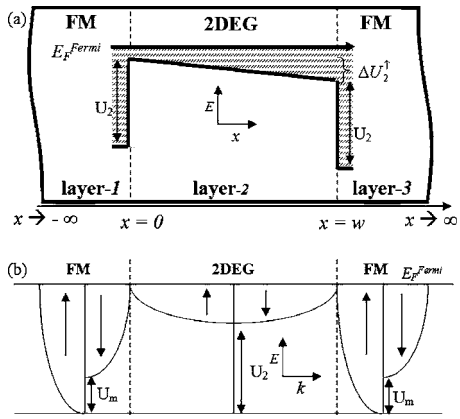

FIG. 2. (a) Schematic diagram showing the energy barrier in the hybrid HEMT structure. Only the spin-up component is shown. (b) Schematic band diagram of the structure showing the origin of U_2 and U_m.

$$\mathrm{MR} \equiv \frac{R_{AP} - R_P}{R_P} = \frac{\Delta\mu_0^{AP} - \Delta\mu_0^{P}}{\Delta\mu_0^{P}} = \frac{\alpha_F[(1-\alpha_F^2)(\Delta U_2^{\uparrow} - \Delta U_2^{\downarrow}) + 4ej_F\alpha_F\lambda_F\rho_F]}{(1-\alpha_F^2)[(1+\alpha_F)\Delta U_2^{\uparrow} + (1-\alpha_F)\Delta U_2^{\downarrow} + 4ej_F\lambda_F\rho_F]}, \tag{10}$$

where R_{AP} (R_P) refers to the overall resistance in the AP (P) configuration and $\Delta\mu_0^{P,AP} = \mu_0^{P,AP}(x = -\lambda_F) - \Delta\mu_0^{P,AP}(x = w + \lambda_F)$. μ_0 is the linear (Ohmic) component of the electrochemical potential, which is the equilibrium spin-independent component of either $\mu_{\uparrow}(x)$ or $\mu_{\downarrow}(x)$.

B. Ballistic transport model within the 2DEG

Next we model the electron transport in layer 2—i.e., the 2DEG layer. We assume the electron's mean free path to be longer than the 2DEG layer width, so that electron conduction can be described by a ballistic spin-dependent transmission model. We consider the parabolic-band effective-mass approximation, so that (by referring to Fig. 2), the Schrödinger equation for layers 1–3 can, respectively, be written as

$$-\frac{\hbar^2}{2m_F}\frac{\partial^2\Psi_1^{\uparrow,\downarrow}(x)}{\partial(x)} + U_1^{\uparrow,\downarrow}\Psi_1^{\uparrow,\downarrow}(x) = (E_F^{Fermi} + \delta\mu_1^{\uparrow,\downarrow})\Psi_1^{\uparrow,\downarrow}(x), \tag{11a}$$

$$-\frac{\hbar^2}{2m_S}\frac{\partial^2\Psi_2^{\uparrow,\downarrow}(x)}{\partial(x)} + \left(U_2 - \frac{\Delta U_2^{\uparrow,\downarrow}}{w}x\right)\Psi_2^{\uparrow,\downarrow}(x) = E_F^{Fermi}\Psi_2^{\uparrow,\downarrow}(x), \tag{11b}$$

$$-\frac{\hbar^2}{2m_F}\frac{\partial^2\Psi_3^{\uparrow,\downarrow}(x)}{\partial(x)} + U_3^{\uparrow,\downarrow}\Psi_3^{\uparrow,\downarrow}(x) = (E_F^{Fermi} + \delta\mu_3^{\uparrow,\downarrow})\Psi_3^{\uparrow,\downarrow}(x). \tag{11c}$$

For the FM layers, the above equations [i.e., Eqs. (11a) and (11c)] are applicable only at the interfacial regions ($x = 0$ and

$x=w$), where ballistic transmission occurs between the FM and 2DEG layers. Away from the interfaces—i.e., within the bulk FM—the electron transport is more accurately described by the spin drift-diffusion equations (2) and (3). The potential energies in the FM regions in the P configuration are given by $U_1^{\uparrow}=0$, $U_1^{\downarrow}=U_m$, $U_3^{\uparrow}=-\Delta U_2^{\uparrow}$, and $U_3^{\downarrow}=U_m-\Delta U_2^{\downarrow}$, where U_m is the energy difference between majority and minority spins due to the molecular magnetic field within the FM material (see, e.g., the two-band model of Ref. 41) and $\Delta U_2^{\uparrow(\downarrow)}$ is the potential energy drop across the 2DEG for spin-up (-down) electrons, respectively. In the AP configuration, we assume that the magnetization of layer 3 is reversed. Thus, in layer 3, the potential energy terms for the two spin orientations are interchanged, i.e., $U_3^{AP\uparrow}=U_m-\Delta U_2^{\uparrow}$ and $U_3^{AP\downarrow}=-\Delta U_2^{\downarrow}$. As shown in Fig. 2(b), U_2 in Eq. (11c) is the shift in potential energy so as to align the 2DEG Fermi level with the Fermi level of the FM layers. Thus, $U_2=E_F^{Fermi}-E_S^{Fermi}$, where E_F^{Fermi} and E_S^{Fermi} are the equilibrium Fermi levels of FM and 2DEG layers, respectively. m_F and m_S are the effective electron mass in the FM and 2DEG layers, respectively, while $\delta\mu_{1(3)}^{\uparrow,\downarrow}$ represents the nonlinear part of the electrochemical potential at the left (right) FM-2DEG interface. This nonlinear component is the deviation of the electrochemical potentials of the two spin channels $\mu^{\uparrow,\downarrow}$ from the Ohmic electrostatic potential, due to spin accumulation at the interface. The relationship between $\delta\mu_{1,3}^{\uparrow,\downarrow}$ and the spin accumulation $\Delta\mu_{1,3}$ of Eq. (4) is given by $\delta\mu_1^{\uparrow}+\delta\mu_1^{\downarrow}=\Delta\mu_1(0)$ and $\delta\mu_3^{\uparrow}+\delta\mu_3^{\downarrow}=\Delta\mu_3(w)$, respectively. Solving the above Schrödinger equation yields the following electron wave function in each region:

$$\Psi_1^{\uparrow,\downarrow}(x)=C_1^{\uparrow,\downarrow}\exp(ik_1^{\uparrow,\downarrow})+D_1^{\uparrow,\downarrow}\exp(-ik_1^{\uparrow,\downarrow}), \tag{12a}$$

$$\Psi_2^{\uparrow,\downarrow}(x)=C_2^{\uparrow,\downarrow}\mathrm{Ai}\left[\frac{(E_F^{Fermi}-U_2)w+\Delta U_2^{\uparrow,\downarrow}x}{\Delta U_2^{\uparrow,\downarrow}}\left(\frac{2m_S\Delta U_2^{\uparrow,\downarrow}}{w\hbar^2}\right)^{1/3}\right]+D_2^{\uparrow,\downarrow}\mathrm{Bi}\left[\frac{(E_F^{Fermi}-U_2)w+\Delta U_2^{\uparrow,\downarrow}x}{\Delta U_2^{\uparrow,\downarrow}}\left(\frac{2m_S\Delta U_2^{\uparrow,\downarrow}}{w\hbar^2}\right)^{1/3}\right], \tag{12b}$$

$$\Psi_3^{\uparrow,\downarrow}(x)=C_3^{\uparrow,\downarrow}\exp(ik_3^{\uparrow,\downarrow})+D_3^{\uparrow,\downarrow}\exp(-ik_3^{\uparrow,\downarrow}), \tag{12c}$$

where Eq. (12b) is an Airy Function. The wave vectors at the FM layer interfaces are

$$k_{1,3}^{\uparrow,\downarrow}=\frac{\sqrt{2}\sqrt{m_F E_F^{Fermi}+m_F\delta\mu_{1,3}^{\uparrow,\downarrow}-m_F U_{1,3}^{\uparrow,\downarrow}}}{\hbar}. \tag{13}$$

The coefficients $C_{1,2,3}^{\uparrow,\downarrow}$ and $D_{1,2,3}^{\uparrow,\downarrow}$ are determined by applying flux and wave function matching at the FM-2DEG interfaces:

$$\psi_1^{\uparrow,\downarrow}(0)=\psi_2^{\uparrow,\downarrow}(0), \tag{14a}$$

$$\psi_2^{\uparrow,\downarrow}(w)=\psi_3^{\uparrow,\downarrow}(w), \tag{14b}$$

$$\frac{1}{m_F}\frac{d\psi_1^{\uparrow,\downarrow}(x)}{dx}\bigg|_{x=0}=\frac{1}{m_S}\frac{d\psi_2^{\uparrow,\downarrow}(x)}{dx}\bigg|_{x=0}, \tag{14c}$$

$$\frac{1}{m_S}\frac{d\psi_{21}^{\uparrow,\downarrow}(x)}{dx}\bigg|_{x=w}=\frac{1}{m_F}\frac{d\psi_3^{\uparrow,\downarrow}(x)}{dx}\bigg|_{x=w}, \tag{14d}$$

$$D_3^{\uparrow,\downarrow}=0. \tag{14e}$$

Equations (14a) and (14b) are obtained by applying wave function matching at the interfaces. Equations (14c) and (14d) are obtained by applying flux matching at the interfaces. Since there is no reflected wave at the final FM layer (layer 3), Eq. (14e) denotes zero amplitude of the reflected wave there. By solving these equations we obtained the ratio $C_3^{\uparrow,\downarrow}/C_1^{\uparrow,\downarrow}$. The ballistic transmission probability across the 2DEG layer is then given by

$$T^{\uparrow,\downarrow}=\frac{k_3^{\uparrow,\downarrow}}{k_1^{\uparrow,\downarrow}}\left|\frac{C_3^{\uparrow,\downarrow}}{C_1^{\uparrow,\downarrow}}\right|. \tag{15}$$

Assuming perfect ballistic transmission, the (areal) resistance across the 2DEG layer can be obtained from Landauer's formula as

$$R_2^{\uparrow,\downarrow}=\frac{2\pi\hbar}{e^2T^{\uparrow,\downarrow}}n_m A_F, \tag{16}$$

where n_m is the number of transverse modes and A_F is the cross-sectional area (in the y-z plane) of the device. To simplify our analysis, we restrict our analysis to one transverse conductance mode only ($n_m=1$). This may be achieved in practice, e.g., by constricting the FM-SC interface to a narrow channel, so that it acts as a mode filter, which allows only one transverse mode to pass through. We have also neglected any effects arising from Schottky barriers at the FM-2DEG interfaces. This is because the presence of a Schottky barrier, although it may possibly increase the overall MR ratio,[42] is an undesirable feature in practical GaAs/AlGaAs 2DEG heterostructures, for which Ohmic contacts are much preferred.[43]

To complete the transport calculations, we have to unify the ballistic and diffusive transport within the 2DEG and FM layers, respectively. This is performed based on our earlier scheme,[44] in which the link between the two transport regimes is established by considering the spin accumulation component of the potential $\delta\mu^{\uparrow,\downarrow}$. The values of $\delta\mu^{\uparrow,\downarrow}$ at the FM-SC interfaces are determined by the SDD relations [i.e., Eqs. (2) and (4)]. These, in turn, contribute to the kinetic energy of electrons undergoing ballistic transmission at the FM-2DEG interfaces and hence affects $T^{\uparrow,\downarrow}$ across the 2DEG [from Eqs. (13) and (15)]. Additionally, we assume that the conduction electrons are sufficiently equilibrated after undergoing ballistic transmission across the 2DEG, so that the total potential drop experienced by the electrons across the 2DEG is given by $\Delta U_2^{\uparrow,\downarrow}=j_F^{\uparrow,\downarrow}R_2^{\uparrow,\downarrow}$. For simplicity, we have neglected the detailed analysis of thermoballistic current in the equilibration process.[45,46] Conversely, as can be seen from Eqs. (12a), (12b), and (16), $T^{\uparrow,\downarrow}$ itself is also a function of $\Delta U_2^{\uparrow,\downarrow}$. Based on the above interdependence, a self-consistency loop can be established between the ballistic and SDD transport calculations to solve for $T^{\uparrow,\downarrow}$ and hence $R_2^{\uparrow,\downarrow}$

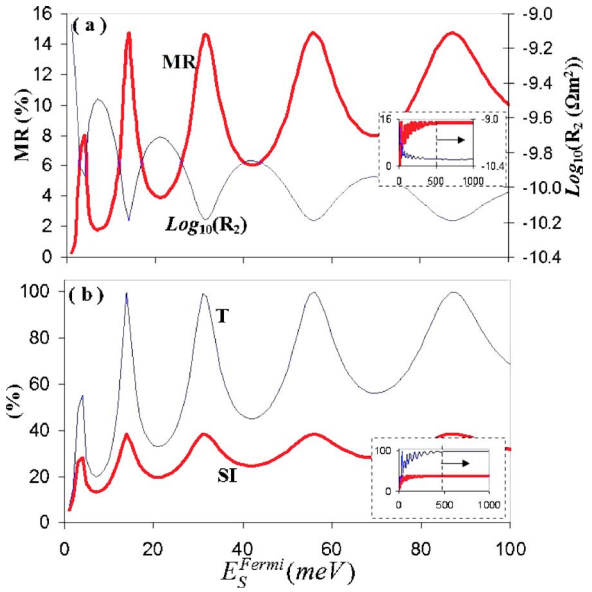

FIG. 3. (Color online) (a) Thick [thin] line shows the MR $[\log_{10}(R_2)]$ variation with change in Fermi energy of the 2DEG. (b) Thick (thin) line shows the variation of the mean transmission probability T (spin injection SI ratio) with the 2DEG Fermi energy. Insets show the variation of parameters over a larger range of E_S^{Fermi} up to $E_S^{Fermi}=1000$ meV. The resonant (oscillatory) behavior disappears for $E_S^{Fermi}>500$ meV. The axis labels for the insets are identical to the main graphs.

across the 2DEG. The self-consistency calculations are performed until the values of $R_2^{\uparrow,\downarrow}$ have converged to better than 0.1% accuracy.

In the numerical calculations, we assume the hybrid structure to be composed of the following materials: FM electrodes of nominally half-metallic Fe_3O_4 and the SC conducting layer consisting of a highly doped n^{++} AlGaAs-GaAs 2DEG. Unless otherwise specified, the following parameter values are assumed: $E_S^{Fermi}=3.5$ meV, $\alpha_F=0.7$, $j_F=1$ A/m^2, $\rho_F=10^{-4}\ \Omega$ m, $A_F=50$ nm$\times 50$ nm (in the y-z plane), $\lambda_F=100$ nm, $m_F=1m_e=9.1\times10^{-31}$ kg, $m_S=0.067m_e$, $E_F^{Fermi}=11.10$ eV, $U_m=0.25$ eV, and $w=40$ nm.

III. RESULTS AND DISCUSSION

Based on the self-consistency transport model described above, we investigated the spin transport behavior in the hybrid FM-2DEG structure. We focus our analysis on the effects of varying the following parameters of the 2DEG layer: (i) Fermi energy (E_S^{Fermi}) and (ii) width (w), and on transport properties such as the MR and SI ratios, 2DEG resistance R_2, and the transmission probability T. Since the transmission curves of both spin-up and -down electrons show similar oscillations with respect to E_S^{Fermi} and w, we have therefore considered the mean transmission probability $T=(T^{\uparrow}+T^{\downarrow})/2$ across the 2DEG layer. The mean value of T is also used in calculating the MR ratio, thus indicating that the oscillatory MR effect originates from both spin channels.

Referring to Fig. 3(a), we obtain a general trend of decreasing resistance of 2DEG layer as the electron energy in the Fermi level, E_S^{Fermi}, is increased. This is due to the fact that electrons with higher kinetic energy can transmit across the 2DEG layer more easily, as shown by the dotted curve in Fig. 3(b). However, the decrease in R_2 is not monotonic, but exhibits an oscillatory behavior with increasing E_S^{Fermi}. This oscillatory behavior is due to the resonant ballistic transport across the 2DEG layer of finite width w. It should be noted that in the ballistic transport, the electron energy is always larger than the potential barrier height U_2 within the 2DEG layer [see Fig. 2(a)]. At the resonant peaks of transmission, T approaches almost perfect transmission of 100%. Noting that R_2 is inversely proportional to electron transmission probability T [see Eq. (16)], the curve for R_2 in Fig. 3(b) thus shows an inverse dependence on E_S^{Fermi} compared to that of T. The oscillatory behavior is, however, suppressed at large values of E_S^{Fermi} exceeding 500 meV, as shown in the insets of Fig. 3.

The MR ratio exhibits an opposite trend, i.e., oscillatory increasing trend with E_S^{Fermi}, compared to R_2 [see Fig. 3(a)]. This may be explained as follows: when the resistance R_2 of the 2DEG layer is higher, the spin-dependent scattering within the FM layers becomes relatively less dominant. Since the spin asymmetry of R_2 is much lower than that in the FM layers, the relative decrease in FM resistivity reduces the overall spin asymmetry of transport across the FM-2DEG structure and thus depresses the MR ratio. The results indicate that we can, in general, improve the MR ratio by increasing the doping density of the SC layer, i.e., increasing the Fermi level within the 2DEG conduction band. More importantly, the strong oscillatory MR behavior can be exploited for certain applications. For instance, by changing E_S^{Fermi} either by changing the 2DEG doping level or by applying an external gate bias, one can induce a large increase in MR. This is especially for low values of $E_S^{Fermi}<20$ meV, where the MR changes from a low of 2% to a high of 17% within $\Delta E_S^{Fermi}\approx 5$ meV.

Next we analyze the effect of increasing 2DEG layer thickness w on the spin-dependent transport. As before, the resonant ballistic transport across the 2DEG results in an oscillatory behavior in T and hence R_2 with changing w, as shown in Fig. 4(a). We assume the range of w considered to be within the mean free path of electrons in the 2DEG. For the parameter values used, the minimum R_2 occurs when the thickness of $w=40$ nm, and this minimum value repeats for every $\Delta w=40$ nm increment in the 2DEG thickness. Due to the inverse relation between MR and R_2, the MR ratio reaches a maximum value at the minimum R_2 and varies with the same period as R_2. The period of oscillation is significantly larger than the MR oscillations seen in MTJs, where Δw is typically $\sim 1-2$ nm.[25,30,35] Another striking difference is the constancy of the amplitude of oscillations in the hybrid FM-2DEG device, as w is varied. By contrast, the amplitude of oscillations in MTJ devices undergoes a rapid (exponential) decrease with w.[25,35] This is because in the MTJ devices, the SPRT effect arises due to charge tunneling and quantum well states within the NM spacer, while in hybrid FM-2DEG devices, it is due to the ballistic transmission of free electrons across the 2DEG. The two differences result in greater practical convenience to modulate the MR ratio in the hybrid device, because (i) the large Δw values mean that it is un-

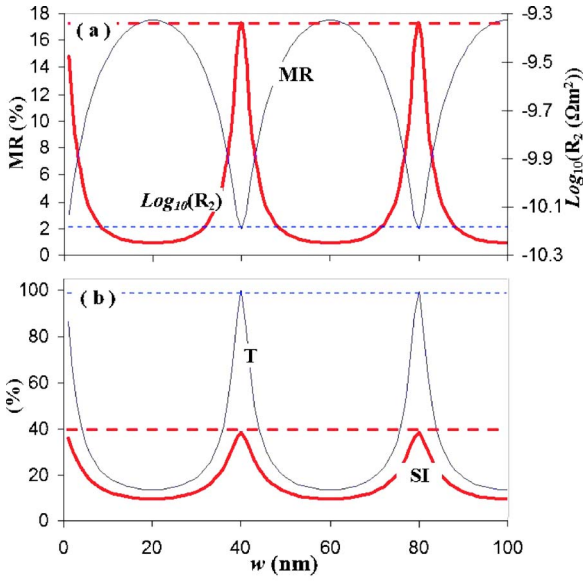

FIG. 4. (Color online) (a) Solid thick [solid thin] line shows the MR $[\log_{10}(R_2)]$ variation with change in SC thickness w. (b) Solid thick (solid thin) line shows the transmission probability T [spin injection (SI)] variation with change in SC thickness w. Here, T refers to the parallel (P) configuration. However, the same trend is also observed for T corresponding to the antiparallel (AP) configuration. Dotted lines indicate the variation of parameters for large E_S^{Fermi}, i.e., $E_S^{Fermi}=500$ meV, where the resonant (oscillatory) behavior is absent.

necessary to achieve high resolution of within a few Å in optimizing w and (ii) the constant amplitude of MR oscillations means that w can be varied without incurring an exponential suppression of MR and conductance. As in Fig. 3, the oscillatory behavior in MR and R_2 decreases with increasing E_S^{Fermi} and is virtually absent at $E_S^{Fermi}=500$ meV, as shown by the dotted lines of Fig. 4.

In addition to the MR ratio, another important parameter for SC-based spintronics devices is the SI efficiency between the FM and SC layers. The SI ratio is defined as the spin polarization of current at the FM source electrode-2DEG interface, i.e.,

$$\mathrm{SI} = (j_{F\uparrow} - j_{F\downarrow})/j_F = 2\beta(x=0) - 1. \tag{17}$$

The variation of SI as a function of E_S^{Fermi} and w is represented by the solid curves in Figs. 3(b) and 4(b), respectively. To explain the SI trend in Fig. 3(b), we note that an increase (decrease) in the 2DEG resistance R_2 and concomitant decrease (increase) in the relative contribution from the FM lead resistances result in an overall increase (decrease) of the spin asymmetry of current through the structure. This, in turn, causes a decrease (increase) in the excess majority spin current, $\Delta j = j_\uparrow - j_\downarrow$, and hence a reduction (increase) in the SI efficiency into the 2DEG. We thus obtain a variation of SI with E_S^{Fermi} [Fig. 3(b)] which is in tandem with that ofMR and in opposing trend to that of R_2. As for the SI trend with the width of the 2DEG layer (w) as plotted in Fig. 4(b), we observe an oscillatory variation of SI with w, which is similar to that of MR. In general, the SI efficiency is significantly higher than the MR ratio and attains a maximum value of 40%, compared to the maximum MR of 16%. This is in agreement with the general approximation that $\mathrm{MR} \approx (\mathrm{SI})^2$ (see, e.g., Ref. 15). The ballistic mode of transport through the 2DEG confers the ability to tune the SI efficiency by modifying the doping concentration or the width of the 2DEG layer, similar to the case of the MR. For instance, at low $E_S^{Fermi} < 20$ meV, one can effect a fourfold increase in SI from 10% to almost 40% within $\Delta E_S^{Fermi} \approx 5$ meV. As for the case of MR, the ballistic mode of transport through the 2DEG confers the ability to tune the SI efficiency by modifying the doping concentration or the width of the 2DEG layer. Ballistic transmission also enables much higher SI and MR ratios to be attained compared to hybrid SC-FM devices operated in the diffusive regime. In the latter, direct spin injection from a FM metal into a SC material suffers from the conductivity mismatch problem, thus yielding a SI efficiency of only $\sim 0.1\%$ and an even smaller MR ratio of $\lesssim 10^{-2}\%$.[15] By contrast, our calculations predict that in the presence of resonant ballistic transport, a maximum SI efficiency approaching 40% is attainable [see Figs. 3(b) and 4(b)]. This compares favorably even with hybrid FM-SC structures which utilize tunnel or Schottky barriers, where a SI efficiency of $\sim 32\%$ has been observed.[21] In addition, in the latter structures which are based on tunneling transport, high MR and SI ratios are usually attained by increasing the tunneling resistance and hence suppressing the device conductance. They also do not exhibit the tunability of MR and SI ratios by external means, which is afforded by the resonant ballistic transport in our device, as described earlier.

IV. CONCLUSION

In conclusion, we have investigated the possibility of achieving spin-polarized resonant transport in a hybrid high-electron-mobilty transistor structure, with source and drain electrodes made of FM material and a channel consisting of a highly doped n^{++} AlGaAs-GaAs 2DEG layer. Our model combines the semiclassical spin-drift diffusive transport inside the FM electrodes, with the ballistic transmission of electrons across the 2DEG layer. Based on a self-consistency scheme, we numerically calculate the spin transport across the hybrid FM-2DEG structure. We focus our analysis on the effects of varying the Fermi level E_S^{Fermi} and width w of the 2DEG layer, on transport properties such as the MR and spin injection (SI) ratios, and on transmission probability T across the 2DEG layer. Our calculations reveal strong oscillatory behavior in both the MR and SI ratios, owing to the ballistic resonant transport across the 2DEG and reminiscent of the spin-polarized resonant tunneling effect, recently observed in metal-based magnetic tunnel junction structures. Our proposed hybrid HEMT structure has several distinct advantages compared to MTJs in practical realization of the SPRT effect in future devices. These include the easy tunability of the MR and SI ratios either by changing the 2DEG doping level

or gate voltage bias (which is not possible in metal-based devices) and the absence of any exponential suppression of MR with barrier thickness. Based on realistic parameter values, we predict that the hybrid HEMT is capable of achieving maximum MR and SI ratios of approximately 20% and 40%, respectively.

[1] G. A. Prinz, Phys. Today **48** (4), 58 (1995).
[2] G. A. Prinz, Science **282**, 1660 (1998).
[3] S. A. Wolf, D. D. Awschalom, R. A. Buhrman, J. M. Daughton, S. von Molnar, M. L. Roukes, A. Y. Chtchelkanova, and D. M. Treger, Science **294**, 1488 (2001).
[4] I. Zutic, J. Fabian, and S. Das Sarma, Rev. Mod. Phys. **76**, 323 (2004).
[5] D. Hagele, M. Oestreich, W. W. Ruhle, N. Nestle, and K. Eberl, Appl. Phys. Lett. **73**, 1580 (1998).
[6] J. M. Kikkawa and D. D. Awschalom, Nature (London) **397**, 139 (1999).
[7] Y. Ohno, D. K. Young, B. Beschoten, F. Matsukura, H. Ohno, and D. D. Awschalom, Nature (London) **402**, 790 (1999).
[8] H. Ohno, D. Chiba, F. Matsukura, T. Omiya, E. Abe, T. Dietl, Y. Ohno, and K. Ohtani, Nature (London) **408**, 944 (2000).
[9] M. Yamanouchi, D. Chiba, F. Matsukura, and H. Ohno, Nature (London) **428**, 539 (2004).
[10] M. Yamanouchi, D. Chiba, F. Matsukura, T. Dietl, and H. Ohno, Phys. Rev. Lett. **96**, 096601 (2006).
[11] S. Datta and B. Das, Appl. Phys. Lett. **56**, 665 (1990).
[12] F. G. Monzon and M. L. Roukes, J. Magn. Magn. Mater. **198**, 632 (1999).
[13] T. Koga, J. Nitta, H. Takayanagi, and S. Datta, Phys. Rev. Lett. **88**, 126601 (2002).
[14] M. Khodas, A. Shekhter, and A. M. Finkel'stein, Phys. Rev. Lett. **92**, 086602 (2004).
[15] G. Schmidt, D. Ferrand, L. W. Molenkamp, A. T. Filip, and B. J. van Wees, Phys. Rev. B **62**, R4790 (2000).
[16] E. I. Rashba, Phys. Rev. B **62**, R16267 (2000).
[17] A. Fert and H. Jaffres, Phys. Rev. B **64**, 184420 (2001).
[18] P. R. Hammar, B. R. Bennett, M. J. Yang, and Mark Johnson, Phys. Rev. Lett. **83**, 203 (1999).
[19] S. Gardelis, C. G. Smith, C. H. W. Barnes, E. H. Linfield, and D. A. Ritchie, Phys. Rev. B **60**, 7764 (1999).
[20] H. J. Zhu, M. Ramsteiner, H. Kostial, M. Wassermeier, H.-P. Schonherr, and K. H. Ploog, Phys. Rev. Lett. **87**, 016601 (2001).
[21] B. T. Jonker, Proc. IEEE **91**, 727 (2003).
[22] R. Fiederling, M. Keim, G. Reuscher, W. Ossau, G. Schmidt, A. Waag, and L. W. Molenkamp, Nature (London) **402**, 787 (1999).
[23] A. Slobodskyy, C. Gould, T. Slobodskyy, C. R. Becker, G. Schmidt, and L. W. Molenkamp, Phys. Rev. Lett. **90**, 246601 (2003).
[24] J. Peralta-Ramos and A. M. Llois, Phys. Rev. B **73**, 214422 (2006).
[25] S. Yuasa, T. Nagahama, and Y. Suzuki, Science **297**, 234 (2002).
[26] A. Vedyayev, N. Ryzhanova, C. Lacroix, L. Giacomoni, and B. Dieny, Europhys. Lett. **39**, 219 (1997).
[27] S. Zhang and P. M. Levy, Phys. Rev. Lett. **81**, 5660 (1998).
[28] J. Mathon and A. Umerski, Phys. Rev. B **60**, 1117 (1999).
[29] J. J. Sun and P. P. Freitas, J. Appl. Phys. **85**, 5264 (1999).
[30] J. S. Moodera *et al.*, Phys. Rev. Lett. **83**, 3029 (1999).
[31] P. LeClair, H. J. M. Swagten, J. T. Kohlhepp, R. J. M. van de Veerdonk, and W. J. M. de Jonge, Phys. Rev. Lett. **84**, 2933 (2000).
[32] J. S. Moodera, T. H. Kim, C. Tanaka, and C. H. de Groot, Philos. Mag. B **80**, 195 (2000).
[33] P. LeClair, J. T. Kohlhepp, H. J. M. Swagten, and W. J. M. de Jonge, Phys. Rev. Lett. **86**, 1066 (2001).
[34] P. LeClair *et al.*, Phys. Rev. B **64**, 100406 (2001).
[35] T. Nozaki, Y. Jiang, Y. Kaneko, A. Hirohata, N. Tezuka, S. Sugimoto, and K. Inomata, Phys. Rev. B **70**, 172401 (2004).
[36] T. Nozaki, N. Tezuka, and K. Inomata, Phys. Rev. Lett. **96**, 027208 (2006).
[37] P. C. van Son, H. van Kempen, and P. Wyder, Phys. Rev. Lett. **58**, 2271 (1987).
[38] T. Valet and A. Fert, Phys. Rev. B **48**, 7099 (1993).
[39] A. Brataas, Y. V. Nazarov, and G. E. W. Bauer, Phys. Rev. Lett. **84**, 2481 (2000).
[40] A. Shpiro, P. M. Levy, and S. Zhang, Phys. Rev. B **67**, 104430 (2003).
[41] J. C. Slonczewski, Phys. Rev. B **39**, 6995 (1989).
[42] T. Hanbicki, O. M. J. van t Erve, R. Magno, G. Kioseoglou, C. H. Li, G. Itskos, R. Mallory, M. Yasar, and A. Petrou, Appl. Phys. Lett. **82**, 4092 (2003).
[43] H. Goronkin, S. Tehrani, T. Remmel, P. L. Fejes, and K. J. Johnson, IEEE Trans. Electron Devices **36**, 281 (1989).
[44] S. Agrawal, M. B. A. Jalil, S. G. Tan, K. L. Teo, and T. Liew, Phys. Rev. B **72**, 075352 (2005).
[45] R. Lipperheide and U. Wille, Phys. Rev. B **72**, 165322 (2005).
[46] An approximate analysis of the effect of thermally induced electron motion is performed by assuming an increase of electron kinetic energy of the order of k_BT above the nominal Fermi level. The calculated results show that the oscillations in the MR ratio, SI efficiency, and other transport parameters with respect to E_S^{Fermi} and the 2DEG width w are still evident, but the amplitude of the oscillations is reduced by about 20–50%. However, the frequency of oscillations with w is increased substantially, thus indicating increased device sensitivity to changes in the 2DEG dimensions.